Cavity QED analysis of an exciton-plasmon hybrid molecule via the generalized nonlocal optical response method

Harini Hapuarachchi[*] and Malin Premaratne[†]
Advanced Computing and Simulation Laboratory (AχL), Department of Electrical and Computer Systems Engineering, Monash University, Clayton, Victoria 3800, Australia

Qiaoliang Bao
Department of Materials Science and Engineering, Monash University, Clayton, Victoria 3800, Australia

Wenlong Cheng
Department of Chemical Engineering, Faculty of Engineering, Monash University, Clayton 3800, Victoria, Australia and The Melbourne Centre for Nanofabrication, 151 Wellington Road, Clayton 3168, Victoria, Australia

Sarath D. Gunapala
Jet Propulsion Laboratory, California Institute of Technology, Pasadena, California 91109, USA

Govind P. Agrawal
The Institute of Optics, University of Rochester, Rochester, New York 14627, USA
(Received 30 January 2017; revised manuscript received 14 May 2017; published 19 June 2017)

A metal nanoparticle coupled to a semiconductor quantum dot forms a tunable hybrid system which exhibits remarkable optical phenomena. Small metal nanoparticles possess nanocavitylike optical concentration capabilities due to the presence of strong dipolar excitation modes in the form of localized surface plasmons. Semiconductor quantum dots have strong luminescent capabilities widely used in many applications such as biosensing. When a quantum dot is kept in the vicinity of a metal nanoparticle, a dipole-dipole coupling occurs between the two nanoparticles giving rise to various optical signatures in the scattered spectra. This coupling makes the two nanoparticles behave like a single hybrid molecule. Hybrid molecules made of metal nanoparticles (MNPs) and quantum dots (QDs) under the influence of an external driving field have been extensively studied in literature, using the local response approximation (LRA). However, such previous work in this area was not adequate to explain some experimental observations such as the size-dependent resonance shift of metal nanoparticles which becomes quite significant with decreasing diameter. The nonlocal response of metallic nanostructures which is hitherto disregarded by such studies is a main reason for such nonclassical effects. The generalized nonlocal optical response (GNOR) model provides a computationally less-demanding path to incorporate such properties into the theoretical models. It allows unified theoretical explanation of observed experimental phenomena which previously seemed to require *ab initio* microscopic theory. In this paper, we analyze the hybrid molecule in an external driving field as an open quantum system using a cavity-QED approach. In the process, we quantum mechanically model the dipole moment operator and the dipole response field of the metal nanoparticle taking the nonlocal effects into account. We observe that the spectra resulting from the GNOR based model effectively demonstrate the experimentally observed size dependent amplitude scaling, linewidth broadening, and resonance shift phenomena compared to the respective LRA counterparts. Then, we provide a comparison between our suggested GNOR based cavity-QED model and the conventional LRA model, where it becomes evident that our analytical model provides a close match to the experimentally suggested behavior. Furthermore, we show that the Rayleigh scattering spectra of the MNP-QD hybrid molecule possess an asymmetric Fano interference pattern that is tunable to suit various applications.

DOI: 10.1103/PhysRevB.95.245419

I. INTRODUCTION

Metal nanoparticles (MNPs) and quantum dots (QDs) whose optical properties are tunable using their size and structure possess a wide array of applications in a variety of fields such as biosensing [1,2], photothermal cancer therapy [3–5], and optoelectronic nanodevices [6–9]. Over the recent years, QDs and MNPs seem to have gained increasing popularity in modern nanophotonics [10–13].

Localized surface plasmons (SPs) are nonpropagating modes of excitations of the conduction band electrons that arise naturally from the scattering problem of a subwavelength metallic nanostructure kept in an oscillating electromagnetic field [14–16]. MNPs much smaller than the wavelength of the incident light (λ) exhibit strong dipolar excitations in the form of localized surface plasmon resonances (LSPRs) which give them a remarkable ability to concentrate optical energy in the nanoscale [17,18]. This ability enables the use

[*]harini.hapuarachchi@monash.edu
[†]malin.premaratne@monash.edu

of individual MNPs as nanoscale optical cavities that are able to focus electromagnetic energy to spots much smaller than λ, overcoming the half-wavelength size limitation of the conventional optical cavities [19,20]. This strong electric field localization can significantly enhance the interactions of MNPs with gain media such as QDs [21].

When a hybrid MNP-QD nanomolecule is optically excited, an additional electric field superposed on the external driving field is experienced by the MNP due to the dipole moment of the optical transitions in the QD. The resulting electric field induces a dipole moment in the MNP which in turn alters the field experienced by the QD leading to a self-feedback [22]. Due to this interaction, artificial hybrid nanomolecules formed by MNPs in proximity with QDs exhibit a variety of fascinating optical properties, which have been thoroughly studied recently [23–26].

The optical response of the MNP plays an important role in determining the behavior of the MNP-QD hybrid molecule. A plethora of studies related to nanoplasmonics and MNP-QD hybrid molecules [19,24,27] utilize the local response approximation (LRA) to model the optical response of the MNP as it quite successfully aids the description of a range of plasmonic phenomena [28]. In the LRA, the nonlocal effects of the MNP's optical response are neglected and the MNP's dipolar polarizability is obtained using a spatially constant, Drude-like permittivity. Nevertheless, LRA has recently been challenged on a number of accounts, one example being its prediction that the resonance energy of surface plasmons in the quasistatic limit is independent of the MNP size. This conflicts with the experimentally observed results [28–32]. The size dependence of the LSPR energy is believed to be a result of the quantum properties of the MNP's free electron gas. These quantum effects enhance further as the particles decrease in size [33]. Modeling the MNP based on *ab initio* approaches such as density-functional theory (DFT) captures such nonclassical effects [34,35]. However, such approaches are computationally demanding. Simpler and computationally less demanding approaches are to surpass the LRA using nonlocal response theories such as the nonlocal hydrodynamic or the generalized nonlocal optical response (GNOR) models [28].

The nonlocal response in metallic nanostructures manifests itself through the presence of longitudinal waves which cause smearing of charge density on the Ångstrom length scale. Due to the nonclassical effects arising as a result of the nonlocal response, nanoplasmonics experiments defy explanations with classical electrodynamics [28–32]. The concept of nonlocal response was first introduced phenomenologically and afterwards based on the semiclassical hydrodynamic Drude model (HDM). The generalized nonlocal optical response (GNOR) model is a recent generalization and an extension of the HDM model, which goes beyond HDM by taking both convection current and electron diffusion phenomena in the MNPs into account [30]. It better captures both size dependent resonance shifts and linewidth broadening of the extinction cross section that occurs with decreasing MNP radius. It has been shown using experiments on dimers with nanometer sized gaps that the GNOR model outlines the experimentally-measured spectra, without the need for invoking the quantum mechanical effect of tunneling [28]. Hence the GNOR model allows unified semiclassical explanations of such known experimental phenomena for both monomers and dimers which previously seemed to require microscopic theory [30]. Moreover, the numerical results obtained in this paper suggest that the GNOR based approach captures the experimentally observed size dependent resonance shifts, linewidth broadening, and the amplitude scaling of the Rayleigh scattering spectra without invoking a need to adopt the Kreibig modification to the plasmon bulk damping rate.

A quantum mechanical analysis of the MNP-QD hybrid molecule which takes the nonlocal effects of the MNP into account is yet to be done. In this paper, we analyze the MNP-QD hybrid molecule in an external driving field using a cavity-QED approach and quantum mechanically model the dipole moment operator and the dipole response field of the metal nanoparticle, taking the nonlocal effects into account using a GNOR based approach.

This paper is organized as follows. We first classically analyze the system using the quasistatic approximation and obtain expressions for the dipole moment and the dipole response field of an MNP kept in the vicinity of a QD under the influence of an external driving field in Sec. II B. In Sec. II C, we quantum mechanically analyze the MNP-QD hybrid molecule using a cavity-QED approach and derive expressions for the surface plasmon mode amplitude and the dipole moment operator element of the MNP under the LRA by comparison with the results obtained in Sec. II B. Additionally, we obtain analytical solutions for the MNP and QD operators of the open quantum system in the weak field limit. In Sec. II E, we modify the equations obtained above for the surface plasmon mode amplitude and the dipole moment operator element of the MNP under the LRA, incorporating the GNOR nonlocal correction to the dipolar polarizability of the MNP. We then discuss the conditions required for the successful applicability of this model. In Sec. II F, we provide an outline of Rayleigh scattering by the hybrid molecule, which will subsequently be used for its numerical analysis. We then numerically analyze the presented cavity QED model using a hybrid molecule containing a silver MNP in Sec. III. We compare and contrast the behavior of the hybrid molecule when the MNP is modeled using the LRA and GNOR dipolar polarizabilities and show that our GNOR based cavity-QED model captures features such as size dependent resonance shifts, amplitude scaling, and linewidth broadening that are not revealed under the LRA, providing a close match to the experimentally suggested behavior [28–32]. Then we present a validity measure for the presented nonlocal cavity-QED model and quantify the predictions for silver. We present a table of dipole moment elements and surface plasmon resonance frequencies for silver at different environment permittivities and MNP radii calculated using our model. We conclude Sec. III by discussing the Fano interference displayed by the MNP-QD hybrid molecule and suggesting a practical application of the phenomenon.

II. FORMALISM

A. Overview of the approach

We consider a hybrid molecule comprised of a spherical, nonmagnetic MNP of radius r_m coupled to a QD of radius r_{qd} embedded in a homogenous dielectric bath with a real positive relative permittivity ϵ_b as shown in Fig. 1. The MNP

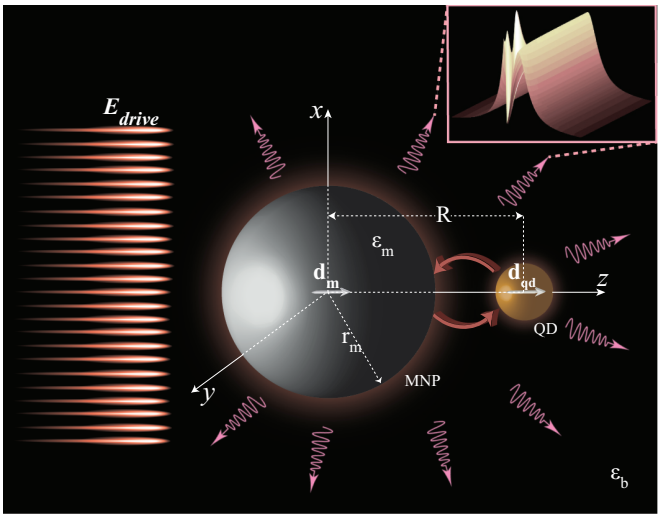

FIG. 1. The schematic diagram of the MNP-QD hybrid molecule in the external driving field. The right insert shows an example Rayleigh scattering spectrum of the hybrid molecule discussed in detail in Secs. II F and III.

and QD are separated by a distance R, allowing no direct tunneling between them ($R - r_m - r_{qd} > 2 \times 10^9$ m) [19]. The hybrid molecule is excited by an external electric field $\boldsymbol{E}_{\mathbf{drive}} = \tilde{\boldsymbol{e}}(E_0^+ e^{-i\omega t} + E_0^- e^{i\omega t})$ where i is the imaginary unit, ω is the angular frequency, and $\tilde{\boldsymbol{e}}$ is a unit vector along or perpendicular to the axis of the hybrid molecule. Throughout our paper, we use the standard sign convention where a positive energy $\hbar\omega$ maps to a positive frequency component, oscillating as $e^{-i\omega t}$ [16]. Therefore, E_0^+ and E_0^- are the respective positive and negative frequency coefficients, where $E_0^+ = E_0^- = E_0$ for the case of $\boldsymbol{E}_{\mathbf{drive}}$. The applied field polarizes both the MNP and the QD, allowing a dipole-dipole coupling between them.

We first analyze the dipolar response of the isolated MNP and then proceed to introduce a Hamiltonian for the hybrid system interacting with the external field, adopting a cavity QED approach. We then model environmental interaction as a Markovian process using a density matrix approach and obtain the solutions for the system operators, after which a compact, computationally less demanding (compared to conventional *ab initio* approaches) correction for the MNP dipolar polarizability is introduced to account for the nonlocal effects in the cavity-QED system. We then analyze the Rayleigh scattering spectra of the system numerically and observe the tunability of the spectra and the Fano line shape using different system parameters.

B. The local response approximation model of MNP-QD hybrid molecule

We initially model the MNP under the LRA [28] where the nonlocal effects are neglected and the relative permittivity of the MNP is described by the spatially constant local dielectric response function $\epsilon_m(\omega)$. The MNP is assumed to be much smaller compared to the wavelength of visible light ($r_m \ll \lambda$), hence the phase of the electric field at any given moment is approximately constant throughout the MNP volume. Additionally, we consider all distances to be small enough for the retardation effects to be ignored, thus justifying the use of the quasistatic approximation [15].

The electric field incident on the MNP is comprised of $\boldsymbol{E}_{\mathbf{drive}}$ and the dipole response field of the QD ($\boldsymbol{E}_{\boldsymbol{qd}}$). The QD is assumed to be sufficiently far apart from the MNP, and therefore the total incident field across the MNP is approximated by a spatially constant planewave $\boldsymbol{E}_{\boldsymbol{in}} \approx \boldsymbol{E}_{\mathbf{drive}} + \boldsymbol{E}_{\boldsymbol{qd}}$. The total spatial electric field distribution ($\boldsymbol{E}$) can be calculated by applying Guass's law to the MNP in the absence of charges, resulting in an expression of the form [15],

$$\boldsymbol{E} \approx \begin{cases} \frac{3\epsilon_b}{\epsilon_m(\omega)+2\epsilon_b}\boldsymbol{E}_{\boldsymbol{in}} & \text{for} \quad r < r_m, \\ \boldsymbol{E}_{\boldsymbol{in}} + \boldsymbol{E}_{\boldsymbol{m}} & \text{for} \quad r \geq r_m, \end{cases} \tag{1}$$

where r is the distance measured from the center of MNP. $\boldsymbol{E}_{\boldsymbol{m}}$ is the response field of the MNP given by,

$$\mathbf{E_m} \approx \frac{\beta_{\mathrm{cm}} r_m^3}{r^3}[3(\boldsymbol{E}_{\boldsymbol{in}}.\tilde{\boldsymbol{r}})\tilde{\boldsymbol{r}} - \boldsymbol{E}_{\boldsymbol{in}}], \tag{2}$$

where $\tilde{\boldsymbol{r}}$ is the unit vector along the axis of the hybrid molecule. β_{cm} is the Clausius Mossotti factor of the MNP in the local response approximation (LRA) [28] denoted by,

$$\beta_{\mathrm{cm}} = \frac{\epsilon_m(\omega) - \epsilon_b}{\epsilon_m(\omega) + 2\epsilon_b}. \tag{3}$$

In the quasistatic regime, the scattering of the incident field ($\boldsymbol{E}_{\boldsymbol{in}}$) by the MNP when $r_m \ll \lambda$ takes the form of a field radiated by a point dipole [36] located at the center of the MNP oriented along the incoming field [15]. Therefore, $\boldsymbol{E}_{\boldsymbol{m}}$ can also be approximated by,

$$\boldsymbol{E}_{\boldsymbol{m}} \approx \frac{1}{4\pi\epsilon_0\epsilon_b r^3}[(3\boldsymbol{d}_{\boldsymbol{m}}.\tilde{\boldsymbol{r}})\tilde{\boldsymbol{r}} - \boldsymbol{d}_{\boldsymbol{m}}], \tag{4}$$

where $\boldsymbol{d}_{\boldsymbol{m}}$ is the dipole moment of the MNP and ϵ_0 is the permittivity of free space. When $\boldsymbol{d}_{\boldsymbol{m}}$ lies along $\tilde{\boldsymbol{r}}$, (4) simplifies to $\boldsymbol{E}_{\boldsymbol{m}} \approx 2\boldsymbol{d}_{\boldsymbol{m}}/(4\pi\epsilon_0\epsilon_b r^3)$ and when $\boldsymbol{d}_{\boldsymbol{m}}$ is perpendicular to $\tilde{\boldsymbol{r}}$, we have $\boldsymbol{E}_{\boldsymbol{m}} \approx -\boldsymbol{d}_{\boldsymbol{m}}/(4\pi\epsilon_0\epsilon_b r^3)$. We define an orientation parameter s_α such that $s_\alpha = 2$ when the external field is polarized along the axis of the hybrid molecule and $s_\alpha = -1$ when the field is polarized perpendicularly to the molecular axis. Using the standard sign convention introduced earlier and with s_α summarizing the orientation, we use (4) to obtain the MNP dipole response field felt by the QD as,

$$E_m^+\Big|_{r\,=\,R} \approx \frac{s_\alpha d_m^+}{4\pi\epsilon_0\epsilon_b R^3}. \tag{5}$$

Similarly, the response field of the QD dipole felt by the MNP is given by $E_{qd}^+|_{r\,=\,0} \approx s_\alpha d_{qd}^+/(4\pi\epsilon_0\epsilon_b R^3)$.

Comparing (2) with (4) and considering only the positive frequency coefficients, we arrive at,

$$d_m^+ \approx 4\pi\epsilon_0\epsilon_b\beta_{\mathrm{cm}} r_m^3 E_{in}^+. \tag{6}$$

Substituting for $\boldsymbol{E}_{\boldsymbol{in}}$ in (6), we obtain the final expression for the MNP dipole moment as,

$$d_m^+ \approx 4\pi\epsilon_0\epsilon_b\beta_{\mathrm{cm}} r_m^3\left(E_0 + \frac{s_\alpha d_{qd}^+}{4\pi\epsilon_0\epsilon_b R^3}\right). \tag{7}$$

We carry forward the equations (5) and (7) to the next section, where we compare them with the expectation values of their respective quantum operator counterparts.

C. Cavity QED model of MNP-QD hybrid molecule

We now quantum mechanically analyze our hybrid molecule in the external driving field (see Fig. 1) with the aid of cavity QED methods. When the QD is irradiated with an external field nearly resonant with the energy gap between its valence and the first conduction bands, a bound electron-hole pair (an exciton) is created [37]. We model our QD as a two level quantum emitter with a dipole moment operator element μ_{qd}. This is a good approximation when studying optical processes at frequencies that are nearly resonant with the frequency corresponding to the lowest excitonic transition energy of the QD [19,38].

The field arising due to the surface plasmons (SPs) in the metal nanoparticle is quantized by associating each mode with a quantum simple harmonic oscillator. For each oscillator mode k, n_k and $|n_k\rangle$ denote the number of surface plasmons and the Fock (or number) state, respectively. For subwavelength particles, SP resonance corresponds to a dipole mode [39]. We assume that only single plasmon excitations occur, therefore only the two states $|0\rangle$ (or vacuum) and $|1\rangle$ of the MNP's dipole mode couple with the QD. We define $\hat{a}^\dagger = |1\rangle\langle 0|, \hat{a} = |0\rangle\langle 1|$ as the plasmonic creation and annihilation operators facilitating the transition between the two Fock states.

We now define the Hamiltonian of our coupled quantum system in the Schrödinger picture as follows:

$$\hat{\mathcal{H}}^{\text{Sch}}_{\text{sys}} = \hat{\mathcal{H}}^{\text{Sch}}_{m} + \hat{\mathcal{H}}^{\text{Sch}}_{qd} + \hat{\mathcal{H}}^{\text{Sch}}_{\text{int}} + \hat{\mathcal{H}}^{\text{Sch}}_{\text{drive}}, \tag{8}$$

where $\hat{\mathcal{H}}^{\text{Sch}}_{m}$ and $\hat{\mathcal{H}}^{\text{Sch}}_{qd}$ are the unperturbed Hamiltonians of the isolated MNP and the QD, respectively. $\hat{\mathcal{H}}^{\text{Sch}}_{\text{int}}$ is the interaction Hamiltonian between the QD and MNP and $\hat{\mathcal{H}}^{\text{Sch}}_{\text{drive}}$ is the interaction Hamiltonian of the hybrid molecule with the external driving field.

By modeling the MNP as a two level quantum system where the initial Schrödinger picture eigenstates $|0\rangle$ and $|1\rangle$ form a complete set of basis states, it can be shown that $\hat{\mathcal{H}}^{\text{Sch}}_{m} = \hbar\omega_m \hat{a}^\dagger \hat{a}$, where the energy of the vacuum state is assumed to be zero. Here, ω_m is the surface plasmon resonance frequency of the MNP, defined as the frequency gap between the two levels $|0\rangle$ and $|1\rangle$.

Similarly, defining $|e\rangle$ and $|g\rangle$ as the basis states of the QD, its state raising and lowering operators are obtained as $\hat{\sigma}^\dagger = |e\rangle\langle g|$ and $\hat{\sigma} = |g\rangle\langle e|$. Defining ω_{qd} as the frequency of the excitonic transition between $|e\rangle$ and $|g\rangle$ and the energy of the ground state to be zero, we obtain $\hat{\mathcal{H}}^{\text{Sch}}_{qd} = \hbar\omega_{qd}\hat{\sigma}^\dagger\hat{\sigma}$.

We then calculate $\hat{\mathcal{H}}^{\text{Sch}}_{\text{int}}$ as the dipole energy of the QD kept in the dipole response field created by the MNP. In the cavity QED treatment of the hybrid molecule, the electric field operator of the surface plasmon $\hat{E}_m$ is approximated by a ring cavity mode [19], where its positive frequency component relates to the plasmon field annihilation operator as [40–42],

$$\hat{E}^+_m \approx i\mathcal{E}\hat{a}. \tag{9}$$

We derive an expression for the coefficient $\mathcal{E}$ towards the end of this section. The optical decay of the QD from the excited state $|e\rangle$ to the ground state $|g\rangle$ is associated with the transition dipole operator $\hat{d}_{qd} = \mu^*_{qd}\hat{\sigma} + \mu_{qd}\hat{\sigma}^\dagger$. With the dipole moment element μ_{qd} assumed real, this simplifies to [27],

$$\hat{d}_{qd} = \mu_{qd}(\hat{\sigma} + \hat{\sigma}^\dagger) = \hat{d}^+_{qd} + \hat{d}^-_{qd}, \tag{10}$$

where $\hat{d}^+_{qd} = \mu_{qd}\hat{\sigma}$ and $\hat{d}^-_{qd} = \mu_{qd}\hat{\sigma}^\dagger$ denote the positive and negative frequency components that will oscillate as $e^{-i\omega t}$ and $e^{i\omega t}$, respectively, when converted to the interaction picture. Following the description of atom-light coupling within the dipole approximation [43,44], $\hat{\mathcal{H}}^{\text{Sch}}_{\text{int}}$ can be written as,

$$\hat{\mathcal{H}}^{\text{Sch}}_{\text{int}} = -\hat{d}_{qd}.\hat{E}_m \approx -(\hat{d}^+_{qd}\hat{E}^-_m + \hat{d}^-_{qd}\hat{E}^+_m), \tag{11}$$

where we have eliminated the nonenergy conserving fast oscillating terms using the rotating wave approximation. Substituting (9) and (10) in (11), we arrive at,

$$\hat{\mathcal{H}}^{\text{Sch}}_{\text{int}} = i\hbar g(\hat{\sigma}\hat{a}^\dagger - \hat{\sigma}^\dagger\hat{a}), \tag{12}$$

where the coupling constant g is defined as [19],

$$g = \frac{\mu_{qd}\mathcal{E}}{\hbar}. \tag{13}$$

We now proceed to derive an expression for the Hamiltonian term $\hat{\mathcal{H}}^{\text{Sch}}_{\text{drive}}$ which results from the dipole interaction of the MNP and QD with E_{drive}. We first define the dipole moment operator of the MNP as,

$$\hat{d}_m = \hat{d}^+_m + \hat{d}^-_m = \mu^*_m\hat{a} + \mu_m\hat{a}^\dagger, \tag{14}$$

where μ_m is the dipole moment element of $\hat{d}_m$. This enables us to write: $\hat{\mathcal{H}}^{\text{Sch}}_{\text{drive}} = -E_{\text{drive}}(\hat{d}_{qd} + \hat{d}_m)$. By substituting for E_{drive}, $\hat{d}_{qd}$, $\hat{d}_m$ and applying the rotating wave approximation, we arrive at,

$$\begin{aligned}\hat{\mathcal{H}}^{\text{Sch}}_{\text{drive}} = &-E_0(\mu_m\hat{a}^\dagger e^{-i\omega t} + \mu^*_m\hat{a}e^{i\omega t})\\ &- E_0\mu_{qd}(\hat{\sigma}^\dagger e^{-i\omega t} + \hat{\sigma}e^{i\omega t}).\end{aligned} \tag{15}$$

Substituting these results in (8) yields the complete expression for the system Hamiltonian in the Schrödinger picture. We then convert it to the interaction picture where the interaction frame rotates at the driving field frequency ω.

We first recast the system Hamiltonian in the Schrödinger picture to the following form,

$$\hat{\mathcal{H}}^{\text{Sch}}_{\text{sys}} = \hat{\mathcal{H}}_0 + \hbar\Delta_m\hat{a}^\dagger\hat{a} + \hbar\Delta_{qd}\hat{\sigma}^\dagger\hat{\sigma} + \hat{\mathcal{H}}^{\text{Sch}}_{\text{int}} + \hat{\mathcal{H}}^{\text{Sch}}_{\text{drive}}, \tag{16}$$

where $\hat{\mathcal{H}}_0 = \hbar\omega\hat{a}^\dagger\hat{a} + \hbar\omega\hat{\sigma}^\dagger\hat{\sigma}$, and the two detunings of the MNP and QD with E_{drive} are given the notations $\Delta_m = (\omega_m - \omega)$ and $\Delta_{qd} = (\omega_{qd} - \omega)$, respectively. The interaction picture Hamiltonian in a frame rotating at frequency ω is defined as [45],

$$\hat{\mathcal{H}}^{\text{Int}}_{\text{sys}} = \hat{\mathcal{U}}^\dagger_0\hat{\mathcal{V}}\hat{\mathcal{U}}_0, \tag{17}$$

where $\hat{\mathcal{U}}_0 = e^{-i\hat{\mathcal{H}}_0 t/\hbar}$ and $\hat{\mathcal{V}} = \hat{\mathcal{H}}^{\text{Sch}}_{\text{sys}} - \hat{\mathcal{H}}_0$.

Simplification of (17) results in the complete expression for the system Hamiltonian in the interaction picture:

$$\begin{aligned}\hat{\mathcal{H}}^{\text{Int}}_{\text{sys}} = &\hbar\Delta_m\hat{a}^\dagger\hat{a} + \hbar\Delta_{qd}\hat{\sigma}^\dagger\hat{\sigma} + i\hbar g(\hat{a}^\dagger\hat{\sigma} - \hat{a}\hat{\sigma}^\dagger)\\ &- E_0(\hat{d}_m + \hat{d}_{qd}).\end{aligned} \tag{18}$$

$\hat{\mathcal{H}}_{\rm sys}^{\rm Int}$ possesses dressed eigenstates [46] which govern the behavior of the hybrid system.

The above Hamiltonian describes a closed quantum system where we have not yet taken the effects of the environment or the reservoir into account. However, the system couples with the environment forming an open quantum system with irreversible dynamics. This interaction is modeled as a Markovian process [47].

The full quantum dynamics of the coupled nanosystem can be derived using the following master equation for the interaction picture density operator [19,25],

$$\frac{\partial}{\partial t}\hat{\rho} = \frac{i}{\hbar}\left[\hat{\rho},\hat{\mathcal{H}}_{\rm sys}^{\rm Int}\right] + \hat{\mathcal{L}}_{qd} + \hat{\mathcal{L}}_{m}, \tag{19}$$

where the Liouvillian terms $\hat{\mathcal{L}}_{qd}$ and $\hat{\mathcal{L}}_{m}$ are given by [19,25,47],

$$\hat{\mathcal{L}}_{qd} = \frac{\gamma_{qd}}{2}(2\hat{\sigma}\hat{\rho}\hat{\sigma}^{\dagger} - \hat{\sigma}^{\dagger}\hat{\sigma}\hat{\rho} - \hat{\rho}\hat{\sigma}^{\dagger}\hat{\sigma}), \tag{20a}$$

$$\hat{\mathcal{L}}_{m} = \frac{\gamma_{m}}{2}(2\hat{a}\hat{\rho}\hat{a}^{\dagger} - \hat{a}^{\dagger}\hat{a}\hat{\rho} - \hat{\rho}\hat{a}^{\dagger}\hat{a}), \tag{20b}$$

where the Markovian interaction with the reservoirs determines the decay rates γ_{qd} and γ_{m} for the QD exciton and the MNP surface plasmon, respectively [19].

The expectation value of an observable $\hat{Q}$ can be obtained using the trace of the product of $\hat{\rho}$ and $\hat{Q}$ as $\langle\hat{Q}\rangle = {\rm Tr}[\hat{\rho}\hat{Q}]$ [48]. Using this claim, we intend to obtain the equation of motion of $\langle\hat{a}\rangle$ in the interaction picture as,

$$\frac{\partial}{\partial t}\langle\hat{a}\rangle = \frac{\partial}{\partial t}{\rm Tr}[\hat{a}\hat{\rho}] = {\rm Tr}\left[\frac{\partial}{\partial t}(\hat{a}\hat{\rho})\right] = {\rm Tr}\left[\hat{a}\frac{\partial}{\partial t}\hat{\rho}\right]. \tag{21}$$

We insert (18) in (19) and get the trace of the entire expression multiplied by $\hat{a}$ which yields:

$$\frac{\partial}{\partial t}\langle\hat{a}\rangle = {\rm Tr}\left[\hat{a}\left(\frac{i}{\hbar}\left[\hat{\rho},\hat{\mathcal{H}}_{\rm sys}^{\rm Int}\right] + \hat{\mathcal{L}}_{qd} + \hat{\mathcal{L}}_{m}\right)\right]. \tag{22}$$

Assuming the QD and MNP operators commute and using bosonic commutator relations for the MNP operators together with the cyclic property of trace, we simplify (22) to obtain,

$$\frac{\partial}{\partial t}\langle\hat{a}\rangle = -\mathcal{D}_{m}\langle\hat{a}\rangle + g\langle\hat{\sigma}\rangle + \mathcal{M}_{m}, \tag{23}$$

where $\mathcal{D}_{m} = (i\Delta_{m} + \gamma_{m}/2)$ and $\mathcal{M}_{m} = i\mu_{m}E_{0}/\hbar$. Solving (23) for the steady state using $\frac{\partial}{\partial t}\langle\hat{a}\rangle = 0$, we obtain,

$$\langle\hat{a}\rangle = (g\langle\hat{\sigma}\rangle + \mathcal{M}_{m})/\mathcal{D}_{m}. \tag{24}$$

Similarly, as $\langle\hat{\sigma}\rangle = {\rm Tr}\,[\hat{\sigma}\hat{\rho}]$ we write,

$$\frac{\partial}{\partial t}\langle\hat{\sigma}\rangle = {\rm Tr}\left[\hat{\sigma}\left(\frac{i}{\hbar}\left[\hat{\rho},\hat{\mathcal{H}}_{\rm sys}^{\rm Int}\right] + \hat{\mathcal{L}}_{qd} + \hat{\mathcal{L}}_{m}\right)\right]. \tag{25}$$

Using the definitions of $\hat{\sigma}$, $\hat{\sigma}^{\dagger}$ and the orthogonality relation of $|e\rangle$, $|g\rangle$ in the simplification of (25) we arrive at the equation of motion for $\langle\hat{\sigma}\rangle$ as,

$$\frac{\partial}{\partial t}\langle\hat{\sigma}\rangle = -\mathcal{D}_{qd}\langle\hat{\sigma}\rangle - (1 - 2\langle\hat{\sigma}^{\dagger}\hat{\sigma}\rangle)(g\langle\hat{a}\rangle - \mathcal{M}_{qd}), \tag{26}$$

where $\mathcal{D}_{qd} = (i\Delta_{qd} + \gamma_{qd}/2)$ and $\mathcal{M}_{qd} = i\mu_{qd}E_{0}/\hbar$. In the semiclassical formalism where the fields are well defined (noise free), the expectation values of the products of MNP and QD operators are separable [21]. The latter property was utilized in arriving at the result in (26).

For weak fields where the excitonic populations are minute ($\langle\hat{\sigma}^{\dagger}\hat{\sigma}\rangle \ll 1$) [19], we obtain the coupled expression for $\langle\hat{\sigma}\rangle$ at steady state as,

$$\langle\hat{\sigma}\rangle \approx (-g\langle\hat{a}\rangle + \mathcal{M}_{qd})/\mathcal{D}_{qd}. \tag{27}$$

Solving the two coupled equations (24) and (27), and defining $\mathcal{D} = \mathcal{D}_{m}\mathcal{D}_{qd}$, we obtain the decoupled analytical solutions for $\langle\hat{a}\rangle$ and $\langle\hat{\sigma}\rangle$ for weak fields, at steady state:

$$\langle\hat{a}\rangle \approx \frac{\mathcal{M}_{m}\mathcal{D}_{qd} + g\mathcal{M}_{qd}}{\mathcal{D} + g^{2}}, \tag{28a}$$

$$\langle\hat{\sigma}\rangle \approx \frac{\mathcal{M}_{qd}\mathcal{D}_{m} - g\mathcal{M}_{m}}{\mathcal{D} + g^{2}}. \tag{28b}$$

This is one of the main results in this section.

We then proceed to obtain expressions for the plasmon field amplitude $\mathcal{E}$ and the dipole matrix element μ_{m}. If the electric field operator is replaced with its mean value, we obtain the classical electric field that satisfies the Maxwell's equations [49]. Note that $\langle\hat{a}\rangle$ in (28a) is the expectation value of the Schrödinger picture annihilation operator, obtained using the interaction picture density matrix. Hence, $\langle\hat{a}\rangle$ yields the slowly varying amplitude of the expectation value of the interaction picture annihilation operator, $\langle\hat{a}_{I}(t)\rangle = \langle\hat{a}\rangle e^{-i\omega t}$. Similarly, for the QD, $\langle\hat{\sigma}_{I}(t)\rangle = \langle\hat{\sigma}\rangle e^{-i\omega t}$. Thus equating classical positive electric field coefficient of the surface plasmon field felt by the QD in (5), with the expectation value of the relevant quantum operator in (9), we obtain: $E_{m}^{+}|_{r\,=\,R} = \langle\hat{E}_{m}^{+}\rangle = i\mathcal{E}\langle\hat{a}\rangle$. Similarly, from the expectation value of (10), we obtain $d_{qd}^{+} = \langle\hat{d}_{qd}^{+}\rangle = \mu_{qd}\langle\hat{\sigma}\rangle$.

Substituting for $E_{m}^{+}|_{r\,=\,R}$ using (5) and (7), for $\langle\hat{a}\rangle$ using (24) and by separately equating the MNP field components due to the QD and $E_{\rm drive}$, we arrive at the following:

$$\mathcal{E} = \frac{s_{\alpha}}{R^{3}}\sqrt{\frac{\beta_{\rm cm}r_{m}^{3}\hbar\mathcal{D}_{m}}{4i\pi\epsilon_{0}\epsilon_{b}}}, \tag{29a}$$

$$\mu_{m} = -\sqrt{4i\pi\epsilon_{0}\epsilon_{b}\,\beta_{\rm cm}r_{m}^{3}\hbar\mathcal{D}_{m}}. \tag{29b}$$

We then use (29b) and (24) to obtain an expression for $-\mu_{m}\langle\hat{a}\rangle$ and compare the result with (7) as,

$$-\mu_{m}\langle\hat{a}\rangle = 4\pi\epsilon_{0}\epsilon_{b}\beta_{\rm cm}r_{m}^{3}\left(E_{0} + \frac{s_{\alpha}d_{qd}^{+}}{4\pi\epsilon_{0}\epsilon_{b}R^{3}}\right) = d_{m}^{+}. \tag{30}$$

However, we note that the expectation value of (14) states that: $d_{m}^{+} = \langle\hat{d}_{m}^{+}\rangle = \mu_{m}^{*}\langle\hat{a}\rangle$. Therefore, $-\mu_{m} = \mu_{m}^{*}$ is the necessary condition for a given MNP to satisfy this cavity QED model. In the following section, we derive an approximate expression for μ_{m} of metals exhibiting good plasmonic properties that will meet this criteria.

D. Approximations for $\mathcal{E}$ and μ_{m} of good plasmonic materials

We start this section with an overview of good plasmonic materials that will be useful in our subsequent derivations. A necessary condition for the existence of SPs is ${\rm Re}\,[\epsilon_{m}(\omega)] \in$

$\mathbb{R}^-$ [50]. Moreover, a material shows good plasmonic properties when [17],

$$\mathrm{Im}\,[\epsilon_m(\omega)] \ll -\,\mathrm{Re}\,[\epsilon_m(\omega)]. \tag{31}$$

The (complex) polarizability α of the MNP in the LRA is given by $\alpha = 4\pi r_m^3 \beta_{\mathrm{cm}}$ [15], where β_{cm} is the Clausius Mossotti factor given by (3). It can be seen that the polarizability experiences a resonant enhancement when $|\epsilon_m(\omega) + 2\epsilon_b|$ is a minimum. For small $\mathrm{Im}[\epsilon_m(\omega)]$, around the resonance, this simplifies to the Frölich condition in the LRA [15,17],

$$\mathrm{Re}\,[\epsilon_m(\omega_m)] \approx -2\epsilon_b. \tag{32}$$

The magnitude of α at resonance is limited by the incomplete vanishing of its denominator, since $\mathrm{Im}[\epsilon_m(\omega)] \neq 0$.

The rate of energy loss from the SP mode is proportional to $\mathrm{Im}\,[\epsilon_m(\omega)]$ [51]. This leads to a finite lifetime of the SPs leading to a near-resonance decay rate [17,19],

$$\gamma_m \approx 2\eta\,\mathrm{Im}\,[\epsilon_m(\omega_m)], \tag{33}$$

where,

$$\eta = \left(\frac{\mathrm{d}\,\mathrm{Re}\,[\epsilon_m(\omega)]}{\mathrm{d}\,\omega}\right)^{-1}_{\omega=\omega_m}. \tag{34}$$

When the dielectric losses are relatively small (which is applicable to the entire plasmonic region of noble metals), the Kramers-Kronig relations for $\epsilon_m(\omega)$ [17] predicts that $\eta > 0$.

Applying (31), (32), and (33) in (29a) and (29b) when $\Delta_m \approx 0$, we obtain:

$$\mathcal{E} \approx \frac{s_\alpha}{R^3}\sqrt{\frac{3\hbar\eta r_m^3}{4\pi\epsilon_0}}, \tag{35a}$$

$$\mu_m \approx -i\epsilon_b\sqrt{12\pi\epsilon_0\eta r_m^3\hbar}, \tag{35b}$$

where $-\mu_m \approx \mu_m^*$ and hence $d_m^+ \approx \mu_m^*\langle\hat{a}\rangle$. Note that we have corrected the equations in [19] that correspond to (30) and (35b) above.

E. The nonlocal correction

In our discussion so far, we assumed that the MNP of our hybrid molecule possesses a spatially constant local dielectric response. Such responses are well described by a classical Drude-like dielectric function [28,52,53],

$$\epsilon_m(\omega) = \epsilon_{\mathrm{core}}(\omega) - \frac{\omega_p^2}{\omega(\omega + i\gamma)}, \tag{36}$$

where ω_p is the bulk plasmon frequency, γ is the relaxation constant of the bulk material, and $\epsilon_{\mathrm{core}}(\omega)$ is the response from the bound electrons. In cases where interband effects are absent and only the conduction band electrons account for the optical properties of the material, we can safely assume that $\epsilon_{\mathrm{core}} = 1$. However, interband transitions play an important role when determining the optical properties of common plasmonic materials, such as gold and silver. In such cases, $\epsilon_{\mathrm{core}}(\omega)$ can be determined using an experimentally measured, bulk dielectric function $\epsilon_{\mathrm{exp}}(\omega)$ (such as the data set given by Johnson and Christy [54]) using the recipe $\epsilon_{\mathrm{core}}(\omega) = \epsilon_{\mathrm{exp}}(\omega) + \omega_p^2/(\omega(\omega + i\gamma))$ [28].

The energy (or the frequency) of surface plasmon resonances in the MNP is determined by its polarizability using the Frölich condition. In the classical LRA above, the polarizability of the MNP at a given point was modeled to be locally related to the electric field. Conversely, nonlocal electrodynamics partially account for the quantum mechanical effects of the MNP free electron gas using a spatially nonlocal dielectric function. Just as the name implies, this captures the spatially nonlocal relationship between the material polarization and the electric field [55], which better explains the SP resonances of the MNP.

Raza *et al.* [31,32] derived a generalized formula for the nonlocal dipolar polarizability of a small spherical MNP in the nonretarded limit, by taking the nonlocal response into account,

$$\alpha^{\mathrm{NL}} = 4\pi r_m^3 \beta_{\mathrm{cm}}^{\mathrm{NL}}, \tag{37}$$

where $\beta_{\mathrm{cm}}^{\mathrm{NL}}$ is the modified nonlocal Clausius Mossotti factor given by,

$$\beta_{\mathrm{cm}}^{\mathrm{NL}} = \frac{\epsilon_m(\omega) - \epsilon_b(1 + \delta_{\mathrm{NL}})}{\epsilon_m(\omega) + 2\epsilon_b(1 + \delta_{\mathrm{NL}})}. \tag{38}$$

The nonlocal correction δ_{NL} is given by [28],

$$\delta_{\mathrm{NL}} = \frac{\epsilon_m(\omega) - \epsilon_{\mathrm{core}}(\omega)}{\epsilon_{\mathrm{core}}(\omega)}\frac{j_1(k_L r_m)}{k_L r_m j_1'(k_L r_m)}, \tag{39}$$

where j_1 is a spherical Bessel function of the first kind of angular-momentum order 1 and j_1' is its first order differential with respect to the argument. The longitudinal wave vector k_L, which is responsible for the nonlocal effects in the MNP, is modeled in the GNOR approach as,

$$k_L^2 = \epsilon_m(\omega)/\xi_{\mathrm{GNOR}}^2(\omega). \tag{40}$$

The frequency dependent function $\xi_{\mathrm{GNOR}}(\omega)$, known as the nonlocal parameter of the GNOR model, is given by,

$$\xi_{\mathrm{GNOR}}^2(\omega) = \frac{\epsilon_{\mathrm{core}}(\omega)[\kappa^2 + \mathrm{D}(\gamma - i\omega)]}{\omega(\omega + i\gamma)}, \tag{41}$$

where

$$\mathrm{D} = \frac{4}{15}\frac{\gamma}{\omega^2 + \gamma^2}v_f^2 \tag{42}$$

is the diffusion parameter of the GNOR model and $\kappa^2 = (3/5)v_F^2$ for $\omega \gg \gamma$ with v_F being the Fermi velocity. It is evident that when $\delta_{\mathrm{NL}} \to 0$, (38) approaches the Clausius Mossotti factor in the LRA given by (3).

By substituting $\beta_{\mathrm{cm}}^{\mathrm{NL}}$ from (38) in place of β_{cm} in (29a) and (29b), we can obtain the exact versions of $\mathcal{E}$ and μ_m with the nonlocal correction. However, for the same reason outlined in Sec. II C, $-\mu_m^{\mathrm{NL}} \approx (\mu_m^{\mathrm{NL}})^*$ criteria must be met for the MNP-QD molecule to be modeled within the cavity QED approach with a reasonable accuracy, where we have defined μ_m^{NL} as the MNP dipole moment operator element in the nonlocal case. Then we show that this criteria is met near resonance for good plasmonic materials when $\mathrm{Re}(1 + \delta_{\mathrm{NL}}) \gg |\,\mathrm{Im}(1 + \delta_{\mathrm{NL}})|$.

The modified Frölich condition where α^{NL} undergoes a resonant enhancement is given by [28],

$$\mathrm{Re}\,[\epsilon_m(\omega_m)] \approx -2\epsilon_b\,\mathrm{Re}\,(1 + \delta_{\mathrm{NL}}), \tag{43}$$

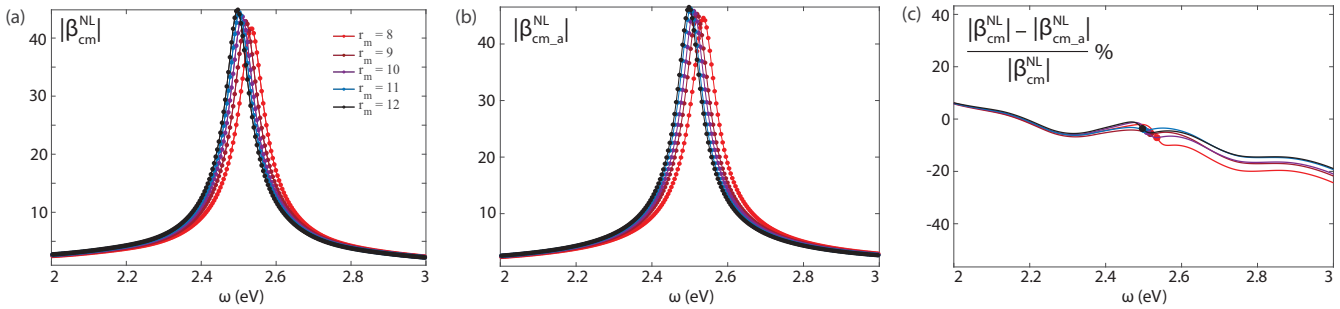

FIG. 2. Comparison of the near-resonant behavior of the GNOR based modified Clausius Mossotti factor presented by Raza *et al.* [28], with its complex Lorentzian approximated form presented in this paper for different MNP radii at $\epsilon_b = 5$. (a) Absolute value of the unapproximated nonlocal Clausius Mossotti factor of Raza *et al.* given by (38). (b) Absolute value of the approximated nonlocal Clausius Mossotti factor $\beta^{\mathrm{NL}}_{\mathrm{cm\_a}}$ given by (45). (c) The percentage error between the absolute values of the unapproximated and approximated (GNOR based) Clausius Mossotti factors given in the previous two subfigures. Percentage errors at resonance are marked on the respective curves in subfigure (c).

for $\mathrm{Re}(1+\delta_{\mathrm{NL}}) \gg |\,\mathrm{Im}(1+\delta_{\mathrm{NL}})|$. When this resonant enhancement occurs, $\mathrm{Re}\,[\epsilon_m(\omega)]$ can be approximated using its first order Taylor expansion near ω_m as,

$$\mathrm{Re}\,[\epsilon_m(\omega)] \approx \mathrm{Re}\,[\epsilon_m(\omega_m)] + (\omega-\omega_m)/\eta. \tag{44}$$

We approximate $\beta^{\mathrm{NL}}_{\mathrm{cm}}$ in (38) around the SP resonance frequency ω_m by a complex Lorentzian using (31), (33), (43), and (44) as follows,

$$\beta^{\mathrm{NL}}_{\mathrm{cm}} \approx 3i\epsilon_b\eta\,\mathrm{Re}(1+\delta_{\mathrm{NL}})/\mathcal{D}_m. \tag{45}$$

Substituting $\beta^{\mathrm{NL}}_{\mathrm{cm}}$ from (45) in (29a) and (29b) yields:

$$\mathcal{E}^{\mathrm{NL}} \approx \frac{s_\alpha}{R^3}\sqrt{\frac{3\hbar\eta r_m^3\,\mathrm{Re}(1+\delta_{\mathrm{NL}})}{4\pi\epsilon_0}}, \tag{46a}$$

$$\mu_m^{\mathrm{NL}} \approx -i\epsilon_b\sqrt{12\pi\epsilon_0\eta r_m^3\hbar\,\mathrm{Re}(1+\delta_{\mathrm{NL}})}. \tag{46b}$$

The equations (45), (46a), and (46b) capture the main results of this paper. It is evident that good plasmonic materials fulfill the $-\mu_m^{\mathrm{NL}} \approx (\mu_m^{\mathrm{NL}})^*$ criteria required by the cavity QED model near resonance, given the condition $\mathrm{Re}(1+\delta_{\mathrm{NL}}) \gg |\,\mathrm{Im}(1+\delta_{\mathrm{NL}})|$ is satisfied. In summary, we highlight the fact that the approximated $\mathcal{E}^{\mathrm{NL}}$ and μ_m^{NL} hold the following relationships with their approximated LRA counterparts.

$$\mathcal{E}^{\mathrm{NL}} \approx \mathcal{E}\sqrt{\mathrm{Re}\,(1+\delta_{\mathrm{NL}})}, \tag{47a}$$

$$\mu_m^{\mathrm{NL}} \approx \mu_m\sqrt{\mathrm{Re}(1+\delta_{\mathrm{NL}})}. \tag{47b}$$

F. Scattering of light by the hybrid molecule

We finally calculate Rayleigh scattering by the hybrid molecule which is valid when the size of the scattering object is much smaller than the wavelength of the incident light [56]. The output scattered light is comprised of coherent and incoherent components. The coherent part is due to elastic Rayleigh scattering where the radiated electromagnetic energy has the same frequency as the incoming field [57]. For low incident light intensities, elastic scattering is dominant. We use this claim to model the Rayleigh scattering by the hybrid molecule, using the cavity QED solutions for the system in the weak field limit given by (28a) and (28b). The coherent part of the scattered intensity is proportional to [19,22],

$$I \approx |d_{qd}^+ + d_m^+|^2 = |\mu_{qd}\langle\hat{\sigma}\rangle + \mu_m^*\langle\hat{a}\rangle|^2, \tag{48}$$

under the LRA. Similarly, for the nonlocal case,

$$I^{\mathrm{NL}} \approx \left|\mu_{qd}^{\mathrm{NL}}\langle\hat{\sigma}\rangle^{\mathrm{NL}} + \left(\mu_m^{\mathrm{NL}}\right)^*\langle\hat{a}\rangle^{\mathrm{NL}}\right|^2, \tag{49}$$

where the superscript NL denotes the relevant quantities calculated using the nonlocally corrected equations. These results will be amply used in the numerical results section that follows.

III. NUMERICAL RESULTS AND DISCUSSION

A. Numerical results

In this section, we numerically analyze the presented cavity QED model for a hybrid molecule, comprised of a QD kept in the vicinity of a silver MNP. Unless stated otherwise, we use an incident field intensity of $1\,\mathrm{W/cm^2}$, $s_\alpha = 2$, $\gamma_{qd} = 50\mu\mathrm{eV}$ and $\mu_{qd} = 33.62$ Debye [19]. The Drude-like dielectric function $\epsilon_m(\omega)$ is obtained from (36) where the bulk parameters for silver used are $\omega_p = 8.99\,\mathrm{eV}$, $\gamma = 0.025\,\mathrm{eV}$, and $v_F = 1.39\times10^6$ m/s [28]. The bound electron response for silver $[\epsilon_{\mathrm{core}}(\omega)]$ is calculated using the measured bulk dielectric values presented by Johnson and Christy in Ref. [54]. We define the detuning between the MNP and QD resonances as $\Delta = \omega_m - \omega_{qd}$.

In Fig. 2, we compare the nonlocal complex Lorentzian approximation of $\beta^{\mathrm{NL}}_{\mathrm{cm}}$ derived in (45) with its unapproximated version in (38) for multiple radii of a subwavelength silver MNP immersed in a medium of $\epsilon_b = 5$. It can be seen that they closely resemble each other near resonance, justifying the use of the approximated version of $\beta^{\mathrm{NL}}_{\mathrm{cm}}$ in the presented cavity QED model, within the given parameter region.

Figures 3(a) and 3(b) show the variation of the coherent Rayleigh scattering curves of the MNP-QD hybrid molecule given by (48) and (49) with varying r_m in the local and nonlocal models, respectively. It is evident that only the model with the GNOR nonlocal correction qualitatively captures the blueshift of resonance energy that occurs with the decreasing particle size, which tallies with the studies done using isolated MNPs in Refs. [31,32]. As our model considers a QD resonance frequency at a fixed detuning from the MNP resonance frequency, the spectrum of the entire molecule shifts to the

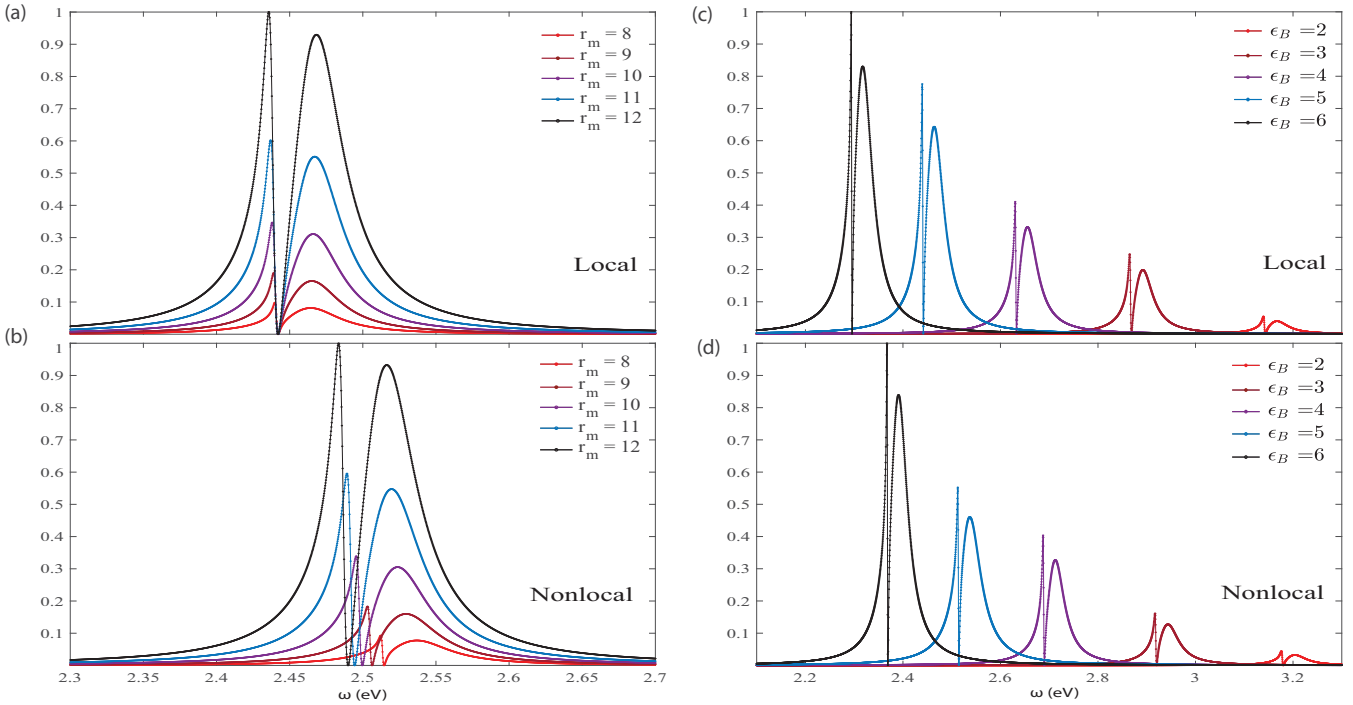

FIG. 3. Variation of coherent Rayleigh scattering spectra of the hybrid molecule with varying r_m and ϵ_b in the local and nonlocal (GNOR) models. Curves are normalized by the largest peak in the respective subfigure. Subfigures (a) and (b) capture the variation of the scattered intensity for different radii at $\epsilon_b = 5$, whereas (c) and (d) capture the scattering intensity variation with the environment permittivity ϵ_b at $r_m = 8$ nm. For all four panels $\Delta = 20$ meV and $R = 14$ nm are used. All figures clearly indicate an asymmetric Fano interference pattern near the resonance frequency of the QD. It can be observed that this asymmetry is tunable using r_m and ϵ_b.

right, following the blueshift of the MNP. The increase in the coherent scattered intensity with the increasing MNP size is captured by both local and nonlocal models.

Figures 3(c) and 3(d) show how the intensity spectra vary with the permittivity of the surrounding medium for the local and nonlocal cases, respectively. Both these cases predict that the resonance frequency and the peak scattered intensity show a high sensitivity to the permittivity of the host medium, a feature that can be exploited in applications such as biosensing [57]. We recall that the resonance frequency is decided by the Frölich condition given by (32) and (43) in the local and nonlocal cases, respectively. Increasing ϵ_b moves the resonance frequency leftwards, along the Drude-like dielectric curve (36) in the optical region for metals such as gold and silver. This frequency redshift with increasing ϵ_b is captured by both local and nonlocal GNOR cases as shown in Figs. 3(c) and 3(d). Additionally, both cases capture the enhancement of the scattered intensity with increasing ϵ_b. However, the resonance frequencies given for the same set of parameters by the local and nonlocal models are seen to be different.

The dependence of the scattered intensity on the orientation parameter s_α is shown in Fig. 4. It also shows how the nonlocal scattered intensity scales in comparison with its local counterpart. This is caused by the introduction of the $\mathrm{Re}(1 + \delta_{\mathrm{NL}})$ component to the approximated expression of μ_m in the nonlocal case. We observe in Figs. 3 and 4 that a sharp enhancement and a suppression of the scattered intensity occur in a small region near the resonance frequency of the QD, due to the respective constructive and destructive interferences of the MNP and QD spectra. Figure 4 shows that this interference effect depends on the external driving field orientation or s_α.

Moreover, we have used Fig. 4 to show that a line broadening effect can be observed in the GNOR spectra in comparison to the respective LRA counterparts. From Fig. 3(b), it can be observed that this line broadening is size dependent. Such size

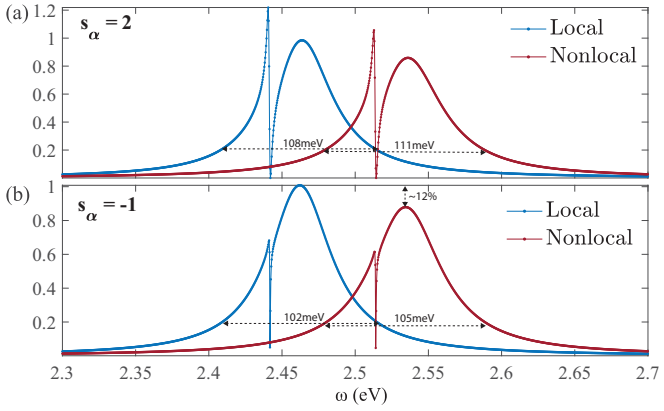

FIG. 4. (a) LRA and GNOR based coherent Rayleigh scattering spectra for $s_\alpha = 2$. (b) Coherent Rayleigh scattering spectra for $s_\alpha = -1$. Other parameters used include $\epsilon_b = 5$, $r_m = 8$ nm, $R = 15$ nm, and $\Delta = 20$ meV. All curves are normalized by the peak intensity of the respective LRA based spectrum for the purpose of amplitude comparison. It can be observed that the Fano interference pattern near the resonance of the QD is influenced by the orientation of the external field.

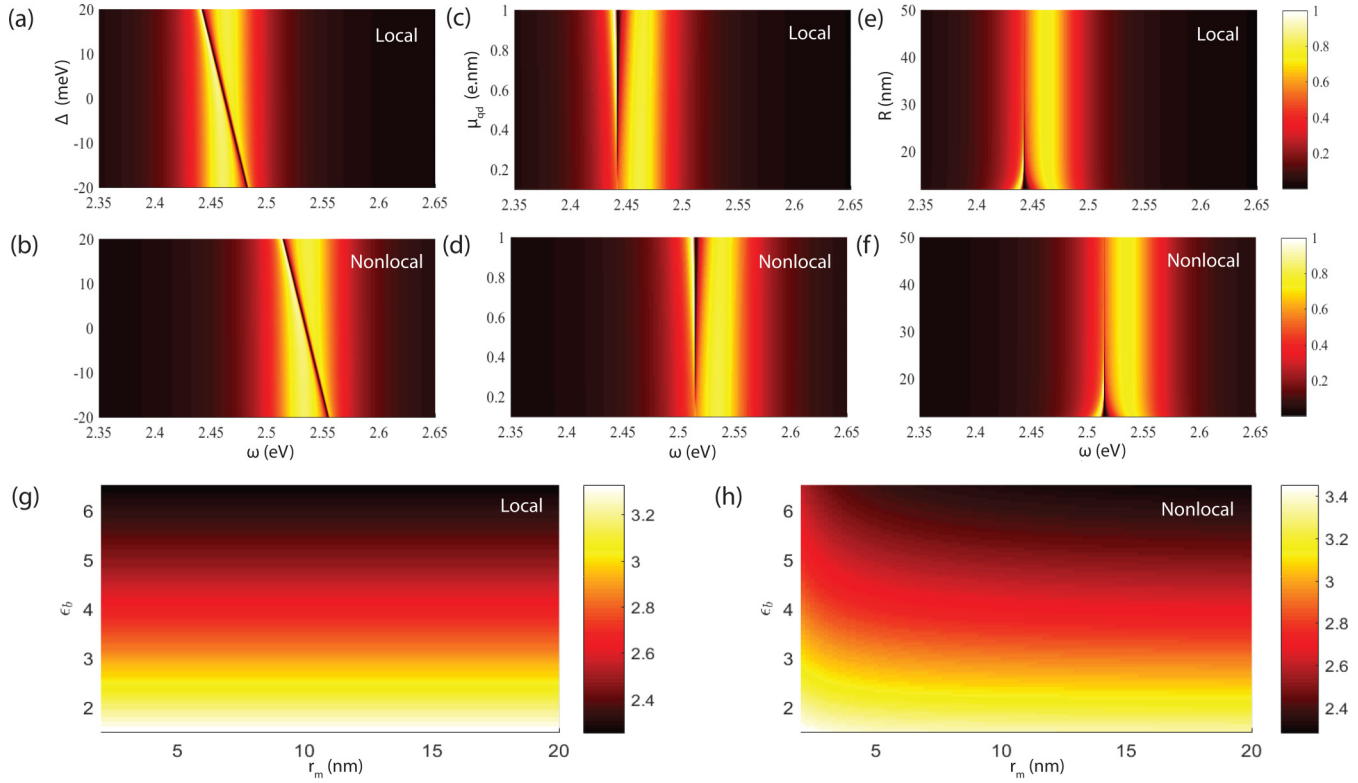

FIG. 5. Subfigures (a)–(f) depict two-dimensional plots for the coherent scattered intensity of the hybrid molecule, normalized by the maximum intensity of each subfigure for $\epsilon_b = 5$ and $r_m = 8$ nm. (a) Shows the scattered intensity variation against Δ and ω when $R = 15$ nm in the LRA. (b) Shows the scattered intensity against Δ and ω for the same set of parameters as in (a) in the nonlocal GNOR model. The subfigures (c) and (d) show, respectively, the local and nonlocal (GNOR) scattering intensities against μ_{qd} and ω. The local and nonlocal (GNOR) scattering intensities against R and ω are shown in (e) and (f), respectively. The subfigures (c)– (f) use $\Delta = 20$ meV and $R = 15$ nm. Subfigure (g) shows the variation of ω_m against r_m and ϵ_b predicted by the LRA, whereas (f) shows the same variation as predicted by the nonlocal GNOR model. From figures (a)– (f) it can be observed that model parameters such as MNP-QD detuning, dipole moment, and distance dramatically affect the Fano lineshape resulting from the interference of the MNP and QD spectra.

dependent damping phenomenon has been reported in several experiments in the past [58–62]. The conventional LRA based model does not account for this phenomenon. The Kreibig approach which phenomenologically modifies the Drude bulk damping parameter as

$$\gamma \to \gamma + \mathrm{A}\frac{v_f}{r_m}, \tag{50}$$

where A is a constant related to the probability of the free electrons scattering off the surface of the particle, has been used by researchers to account for this effect [63]. However, the Kreibig approach fails to account for the size-dependent resonance shifts of the MNP whereas the GNOR based approach successfully captures both effects [28].

Figures 5(a) and 5(b) show two-dimensional plots of the scattered intensity against the MNP-QD detuning Δ and the external driving field frequency ω, given by the local and nonlocal models, respectively. The slanted line across each spectrum shows the movement of the steep enhancement-suppression pattern, seen in Figs. 3 and 4, towards higher frequencies following the movement of the resonance position of the QD along the frequency axis.

Figures 5(c) and 5(d) show scattered intensity variation against μ_{qd} and ω. It is evident that the QD causes a higher enhancement and a suppression in the hybrid molecule spectrum across a wider range of frequencies with increasing μ_{qd}.

The impact of the MNP-QD distance R on the scattered intensity is shown in Figs. 5(e) and 5(f). Figure 5(e) represents LRA and Fig. 5(f) follows the nonlocal GNOR model. It can be observed that the interference effects due to the QD dominate across a larger frequency range when the interparticle distance decreases.

Figure 5(g) shows the variation of the MNP resonance frequency ω_m calculated using the Frölich condition given by (32) in the LRA, against ϵ_b and r_m. It clearly shows that LRA does not capture the radius dependence of the MNP resonance. Figure 5(h), which depicts ω_m given by the nonlocal GNOR Frölich condition (43), readily captures this radius dependence. It is observable that the dependence of ω_m on r_m increases when r_m decreases.

We then do a validity region analysis of our suggested nonlocal cavity QED model for a hybrid molecule containing a silver MNP. As we have already discussed, the successful use of the cavity QED model to analyze the MNP-QD hybrid molecule requires the fulfillment of the condition $-\mu_m^{\mathrm{NL}} \approx (\mu_m^{\mathrm{NL}})^*$. This in turn demands that both the conditions $\mathrm{Im}(\epsilon_m(\omega)) \ll$

TABLE I. Dipole moment operator elements (μ_m^{NL}) and the resonance frequencies (ω_m^{NL}) for a silver MNP, calculated using a nonlocal GNOR based cavity QED approach, against the environment permittivity ϵ_b and the MNP radius r_m. Each cell contains μ_m^{NL} in units of 1×10^{-27}Cm at the top and ω_m^{NL} in eV at the bottom. All dipole moment element values presented carry a tolerance level approximately equal to or less than 0.1. The exact levels of tolerance for the presented dipole moments can be found using $\mathcal{P}_2$ in (51b).

ϵ_B	3 nm	5 nm	7 nm	9 nm	11 nm	13 nm	15 nm	17 nm	19 nm
1.0	$-0.44i$	$-0.98i$	$-1.65i$	$-2.44i$	$-3.31i$	$-4.29i$	$-5.33i$	$-6.44i$	$-7.62i$
	3.55	3.53	3.52	3.51	3.51	3.51	3.51	3.51	3.51
1.5	$-0.70i$	$-1.54i$	$-2.56i$	$-3.73i$	$-5.07i$	$-6.51i$	$-8.09i$	$-9.75i$	$-11.54i$
	3.41	3.37	3.36	3.35	3.35	3.34	3.34	3.34	3.34
2.0	$-0.89i$	$-2.01i$	$-3.37i$	$-4.94i$	$-6.69i$	$-8.62i$	$-10.68i$	$-12.91i$	$-15.23i$
	3.26	3.22	3.21	3.19	3.19	3.19	3.18	3.18	3.18
2.5	$-1.07i$	$-2.28i$	$-3.78i$	$-5.53i$	$-7.50i$	$-9.65i$	$-11.99i$	$-14.48i$	$-17.13i$
	3.13	3.09	3.07	3.06	3.05	3.04	3.04	3.04	3.04
3.0	$-1.19i$	$-2.69i$	$-4.55i$	$-6.71i$	$-9.13i$	$-11.78i$	$-14.66i$	$-17.73i$	$-21.00i$
	3.03	2.97	2.95	2.93	2.93	2.92	2.91	2.91	2.91
3.5	$-1.41i$	$-3.18i$	$-5.29i$	$-7.67i$	$-10.37i$	$-13.29i$	$-16.41i$	$-19.7i$	$-23.32i$
	2.92	2.85	2.82	2.81	2.80	2.79	2.79	2.78	2.78
4.0	$-1.59i$	$-3.27i$	$-5.32i$	$-7.76i$	$-10.46i$	$-13.45i$	$-16.67i$	$-20.16i$	$-23.81i$
	2.82	2.75	2.72	2.71	2.69	2.69	2.68	2.68	2.68
4.5	$-1.59i$	$-3.43i$	$-5.8i$	$-8.56i$	$-11.65i$	$-15.04i$	$-18.69i$	$-22.59i$	$-26.72i$
	2.73	2.66	2.63	2.62	2.60	2.60	2.59	2.59	2.58
5.0	$-1.68i$	$-3.81i$	$-6.35i$	$-9.27i$	$-12.51i$	$-16i$	$-19.8i$	$-23.95i$	$-28.22i$
	2.66	2.58	2.54	2.53	2.51	2.50	2.50	2.50	2.49
5.5	$-1.85i$	$-4.01i$	$-6.57i$	$-9.52i$	$-12.79i$	$-16.31i$	$-20.15i$	$-24.22i$	$-28.69i$
	2.59	2.50	2.47	2.45	2.44	2.43	2.42	2.41	2.41
6.0	$-1.95i$	$-4.1i$	$-6.67i$	$-9.56i$	$-12.86i$	$-16.52i$	$-20.46i$	$-24.65i$	$-29.2i$
	2.52	2.44	2.40	2.38	2.37	2.36	2.35	2.35	2.35
6.5	$-1.99i$	$-4.13i$	$-6.79i$	$-9.94i$	$-13.49i$	$-17.4i$	$-21.66i$	$-26.22i$	$-31.09i$
	2.46	2.38	2.34	2.32	2.31	2.30	2.29	2.29	2.28

$-\mathrm{Re}(\epsilon_m(\omega))$ and $\mathrm{Re}(1+\delta_{\mathrm{NL}}) \gg |\mathrm{Im}(1+\delta_{\mathrm{NL}})|$ are met. We define,

$$\mathcal{P}_1 = \frac{|\mathrm{Im}(1+\delta_{\mathrm{NL}})|}{\mathrm{Re}(1+\delta_{\mathrm{NL}})} \times 100\%, \tag{51a}$$

$$\mathcal{P}_2 = \left| \frac{|\mu_{m\_u}^{\mathrm{NL}}| - |\mu_{m\_a}^{\mathrm{NL}}|}{|\mu_{m\_u}^{\mathrm{NL}}|} \right| \times 100\%, \tag{51b}$$

where $\mu_{m\_u}^{\mathrm{NL}}$ is the unapproximated version of μ_m^{NL} in the nonlocal model obtained by substituting $\beta_{\mathrm{cm}}^{\mathrm{NL}}$ from (38) in (29b), and $\mu_{m\_a}^{\mathrm{NL}}$ is the approximated μ_m^{NL} in the nonlocal model obtained using (46b). We have shown the variation of $\mathcal{P}_1$ and $\mathcal{P}_2$ against the MNP radius and the host medium permittivity for silver in Figs. 6(a) and 6(b), respectively. It can be clearly seen that $\mathcal{P}_2$ is influenced by $\mathcal{P}_1$. However, they do not hold a linear relationship due to the nature of their analytical equations and the incomplete vanishing of $\mathrm{Im}(\epsilon_m(\omega))$ near the surface plasmon resonance of the MNP. $\mathcal{P}_2$ can be used as a *de-facto* tolerance for the presented nonlocal cavity-QED model.

Finally, we present Table I which summarizes the dipole moment operator elements (μ_m^{NL}) and the surface plasmon resonance frequencies (ω_m^{NL}) for silver, calculated using the nonlocal GNOR model equations (46b) and (43) for a range of MNP radii (r_m) and environment permittivities (ϵ_b). All values presented in Table I fall approximately within the region where $\mathcal{P}_2 \leq 0.1$ in Fig. 6.

B. Fano resonance and applications

Unlike the conventional Lorentzian resonance, Fano resonance comprises a distinctly asymmetric shape with a functional form similar to,

$$I_F \propto \frac{(F\Gamma + \omega - \omega_0)^2}{(\omega - \omega_0)^2 + \Gamma^2}, \tag{52}$$

where F is known as the Fano parameter describing the degree of asymmetry, and ω_0 and Γ are parameters denoting the width and the position of the resonance, respectively [64]. The excitations possessed by the QDs are discrete excitons whereas the plasmonic excitations of the MNP comprise a strong continuous spectral response [65]. In our system, an asymmetric Fano behavior arises from the constructive and destructive interference of the narrow discrete resonance of the QD with the broad spectrum of the MNP.

The numerical results presented in Figs. 3–5 clearly indicate that the Rayleigh scattering spectra of the MNP-QD hybrid molecule possess an asymmetric Fano interference pattern which is tunable using different properties of the MNP-QD system such as the constituent sizes, dipole moment, MNP-QD distance, external field orientation, and the environmental permittivity. This tunability of the Fano resonance pattern promises usability of the hybrid system in various applications such as sensing, lasing, switching, and nonlinear and slow-light devices. The inherent sensitivity of the Fano interference pattern of the MNP-QD hybrid molecule renders attraction for a range of practical applications, with the most straightforward

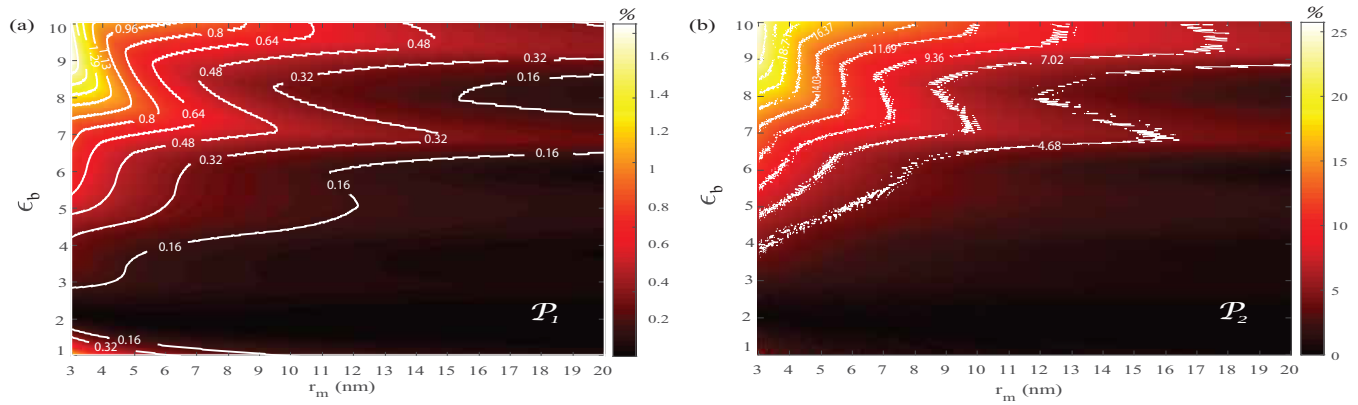

FIG. 6. (a) $\mathcal{P}_1$ calculated using (51a) for silver at the respective resonance frequencies for different MNP radii and environment permittivities. Approximation of $(1+\delta_{\rm NL})$ by $\mathrm{Re}\,(1+\delta_{\rm NL})$ in all the nonlocal (GNOR) equations is justified when $\mathcal{P}_1$ is small and positive. (b) $\mathcal{P}_2$ calculated using (51b) for silver at the respective resonance frequencies for different MNP radii and environment permittivities. $\mathcal{P}_2$ represents the *de-facto* tolerance level for the MNP dipole moment element $\mu_m^{\rm NL}$ given by (46b). Thus, $\mathcal{P}_2$ can be used to assess tolerance levels of the dipole moment elements given in Table I.

application being the usage for development of chemical or biological sensors [64]. As an example, we suggest that the MNP-QD hybrid molecule can be a good candidate for early stage tumor detection as the cancerous tissue possess much higher permittivity than the surrounding normal tissue [66] resulting in a dramatic shift in the observed Fano scattering signature. Furthermore, such tunable signatures can be used in applications such as photothermal cancer therapy [67].

IV. SUMMARY AND CONCLUSION

In this paper, we analyzed the metal nanoparticle-quantum dot (MNP-QD) hybrid molecule in an external driving field using a cavity-QED approach and presented a comprehensive comparison between the behavior suggested by the local response approximation (LRA) and the generalized nonlocal optical response (GNOR) based methods. We have derived expressions for the plasmon field amplitude and the dipole moment operator element of the MNP in the LRA and introduced their nonlocally-corrected versions, outlining the constraints of the model. Additionally, we provided an analytical solution for the cavity-QED system in the weak field regime and numerically studied the scattering spectra of an MNP-QD hybrid molecule comprised of a silver MNP. Optical signatures of the scattering spectra and their variation with the tunable system properties were observed and discussed in this numerical analysis. Many such signatures and their variations against the tunable parameters can in most instances be explained by both the local and nonlocal models. However, the LRA fails to capture some features such as the size dependent resonance shifts, linewidth broadening, and amplitude scaling where the GNOR model succeeds. The nonlocal GNOR model captures the blueshift of resonance energy that occurs with the decreasing particle size, which tallies with experimental studies done using isolated and dimer MNPs. We then provided a numerical quantification for the deviation of the approximated dipole moment of a silver nanoparticle from the exact equation suggested by the cavity QED model. We presented a table summarizing the dipole moment elements of subwavelength silver MNPs with different radii immersed in different background media using the nonlocal GNOR based cavity-QED model. We finally provided a discussion of the Fano signature observed in the Rayleigh scattering spectra of the hybrid system and its potential applications.

ACKNOWLEDGMENTS

H.H. would like to thank the members of AχL at Monash University including D. Weeraddana and S. Mallawaarachchi for their encouragement and support. The work of H.H. is supported by the Monash University Institute of Graduate Research, and the work of M.P., S.D.G., and G.P.A. is supported by the Australian Research Council through its Discovery Grant No. DP140100383. Q.B. would like to acknowledge the support from ARC DP140101501, FT150100450, and CE170100039.

[1] J. N. Anker, W. P. Hall, O. Lyandres, N. C. Shah, J. Zhao, and R. P. Van Duyne, Nat. Mater. **7**, 442 (2008).
[2] J. Homola, S. S. Yee, and G. Gauglitz, Sens. Actuator B-Chem. **54**, 3 (1999).
[3] D. Sikdar, I. D. Rukhlenko, W. Cheng, and M. Premaratne, Nanoscale Res. Lett. **8**, 142 (2013).
[4] D. Sikdar, I. D. Rukhlenko, W. Cheng, and M. Premaratne, Biomed. Opt. Express **4**, 15 (2013).
[5] S. Lal, S. E. Clare, and N. J. Halas, Acc. Chem. Res. **41**, 1842 (2008).
[6] M. I. Stockman, J. Opt. **12**, 024004 (2010).
[7] C. Jayasekara, M. Premaratne, M. I. Stockman, and S. D. Gunapala, J. Appl. Phys. **118**, 173101 (2015).
[8] T. Wijesinghe, M. Premaratne, and G. P. Agrawal, Opt. Express **22**, 2681 (2014).

[9] K. C. Huang, M.-K. Seo, T. Sarmiento, Y. Huo, J. S. Harris, and M. L. Brongersma, Nat. Photon. **8**, 244 (2014).

[10] D. Weeraddana, M. Premaratne, and D. L. Andrews, Phys. Rev. B **92**, 035128 (2015).

[11] C. S. Kumarasinghe, M. Premaratne, S. D. Gunapala, and G. P. Agrawal, Sci. Rep. **6**, 21470 (2016).

[12] C. S. Kumarasinghe, M. Premaratne, Q. Bao, and G. P. Agrawal, Sci. Rep. **5**, 12140 (2015).

[13] C. S. Kumarasinghe, M. Premaratne, S. D. Gunapala, and G. P. Agrawal, Phys. Chem. Chem. Phys. **18**, 18227 (2016).

[14] M. Premaratne and G. P. Agrawal, *Light Propagation in Gain Media: Optical Amplifiers* (Cambridge University Press, New York, 2011).

[15] S. A. Maier, *Plasmonics: Fundamentals and Applications* (Springer Science & Business Media, New York, 2007), Chap. 5.

[16] M. Premaratne and M. I. Stockman, Adv. Opt. Photonics **9**, 79 (2017).

[17] M. I. Stockman, Opt. Express **19**, 22029 (2011).

[18] V. Rivera, E. Marega Jr, and F. Ferri, *Localized Surface Plasmon Resonances: Noble Metal Nanoparticle Interaction with Rare-Earth Ions* (INTECH Open Access Publisher, Rijeka, Croatia, 2012), Chap. 11.

[19] A. Ridolfo, O. Di Stefano, N. Fina, R. Saija, and S. Savasta, Phys. Rev. Lett. **105**, 263601 (2010).

[20] M. Noginov, G. Zhu, A. Belgrave, R. Bakker, V. Shalaev, E. Narimanov, S. Stout, E. Herz, T. Suteewong, and U. Wiesner, Nature (London) **460**, 1110 (2009).

[21] E. Waks and D. Sridharan, Phys. Rev. A **82**, 043845 (2010).

[22] A. V. Malyshev and V. A. Malyshev, Phys. Rev. B **84**, 035314 (2011).

[23] S. Sadeghi, Nanotechnology **21**, 455401 (2010).

[24] R. D. Artuso and G. W. Bryant, Phys. Rev. B **82**, 195419 (2010).

[25] Y. He and K.-D. Zhu, Nanoscale Res. Lett. **7**, 1 (2012).

[26] C. Rupasinghe, I. D. Rukhlenko, and M. Premaratne, Opt. Express **21**, 15335 (2013).

[27] U. Hohenester and A. Trugler, IEEE J. Sel. Top. Quantum Electron. **14**, 1430 (2008).

[28] S. Raza, S. I. Bozhevolnyi, M. Wubs, and N. A. Mortensen, J. Phys. Condens. Matter **27**, 183204 (2015).

[29] J. Tiggesbäumker, L. Köller, K.-H. Meiwes-Broer, and A. Liebsch, Phys. Rev. A **48**, R1749 (1993).

[30] M. Wubs and N. A. Mortensen, *Nonlocal Response in Plasmonic Nanostructures* (Springer, Cham, Switzerland, 2017), Chap. 12.

[31] S. Raza, N. Stenger, S. Kadkhodazadeh, S. V. Fischer, N. Kostesha, A.-P. Jauho, A. Burrows, M. Wubs, and N. A. Mortensen, Nanophotonics **2**, 131 (2013).

[32] S. Raza, W. Yan, N. Stenger, M. Wubs, and N. A. Mortensen, Opt. Express **21**, 27344 (2013).

[33] C. Kumarasinghe, M. Premaratne, and G. P. Agrawal, Opt. Express **22**, 11966 (2014).

[34] J. Zuloaga, E. Prodan, and P. Nordlander, Nano Lett. **9**, 887 (2009).

[35] K. Andersen, K. W. Jacobsen, and K. S. Thygesen, Phys. Rev. B **86**, 245129 (2012).

[36] D. J. Griffiths and R. College, *Introduction to Electrodynamics*, Vol. 3 (Prentice Hall, Upper Saddle River, NJ, 1999), Chap. 3.

[37] A. Davydov, *Theory of Molecular Excitons* (Springer, New York, 2013).

[38] E. Flagg, A. Muller, J. Robertson, S. Founta, D. Deppe, M. Xiao, W. Ma, G. Salamo, and C.-K. Shih, Nat. Phys. **5**, 203 (2009).

[39] D. Sarid and W. Challener, *Modern Introduction to Surface Plasmons: Theory, Mathematica Modeling, and Applications* (Cambridge University Press, New York, 2010), Chap. 9.

[40] R. J. Glauber, Phys. Rev. **130**, 2529 (1963).

[41] Gulfam, Qurrat-ul-Ain, Z. Ficek, and J. Evers, Phys. Rev. A **86**, 022325 (2012).

[42] H. J. Carmichael, Phys. Rev. A **33**, 3262 (1986).

[43] L. Salasnich, *Quantum Physics of Light and Matter* (Springer, Cham, Switzerland, 2014).

[44] D. Weeraddana, M. Premaratne, and D. L. Andrews, Phys. Rev. B **93**, 075151 (2016).

[45] H. M. Wiseman and G. J. Milburn, *Quantum Measurement and Control* (Cambridge University Press, New York, 2009).

[46] M. O. Scully and M. S. Zubairy, *Quantum Optics*, 6th ed. (Cambridge University Press, New York, 1997), Chap. 10.

[47] H.-P. Breuer and F. Petruccione, *The Theory of Open Quantum Systems* (Oxford University Press on Demand, New York, 2002).

[48] K. Blum, *Density Matrix Theory and Applications* (Springer Science & Business Media, Heidelberg, Germany, 2012), Vol. 64, Chap. 2.

[49] K. Sakoda, *Optical Properties of Photonic Crystals*, 2nd ed. (Springer Science & Business Media, Berlin, Germany, 2004), Vol. 80, Chap. 11.

[50] C. Jayasekara, M. Premaratne, S. D. Gunapala, and M. I. Stockman, J. Appl. Phys. **119**, 133101 (2016).

[51] L. D. Landau, J. Bell, M. Kearsley, L. Pitaevskii, E. Lifshitz, and J. Sykes, *Electrodynamics of Continuous Media* (Elsevier, Oxford, England, 2013), Vol. 8.

[52] K. Kolwas and A. Derkachova, Opto-Electron. Rev. **18**, 429 (2010).

[53] W. Zhu, I. D. Rukhlenko, and M. Premaratne, Appl. Phys. Lett. **102**, 011910 (2013).

[54] P. B. Johnson and R.-W. Christy, Phys. Rev. B **6**, 4370 (1972).

[55] J. M. McMahon, S. K. Gray, and G. C. Schatz, Nano Lett. **10**, 3473 (2010).

[56] W. Zhang, A. O. Govorov, and G. W. Bryant, Phys. Rev. Lett. **97**, 146804 (2006).

[57] P. K. Jain, X. Huang, I. H. El-Sayed, and M. A. El-Sayed, Plasmonics **2**, 107 (2007).

[58] U. Kreibig and L. Genzel, Surf. Sci. **156**, 678 (1985).

[59] U. Kreibig and C. v. Fragstein, Z. Phys. **224**, 307 (1969).

[60] M. Gaudry, E. Cottancin, M. Pellarin, J. Lermé, L. Arnaud, J. Huntzinger, J. Vialle, M. Broyer, J. Rousset, M. Treilleux *et al.*, Phys. Rev. B **67**, 155409 (2003).

[61] L. B. Scaffardi and J. O. Tocho, Nanotechnology **17**, 1309 (2006).

[62] K. Kolwas and A. Derkachova, J. Quant. Spectrosc. Radiat. Transfer **114**, 45 (2013).

[63] V. Myroshnychenko, J. Rodríguez-Fernández, I. Pastoriza-Santos, A. M. Funston, C. Novo, P. Mulvaney, L. M. Liz-Marzán, and F. J. G. de Abajo, Chem. Soc. Rev. **37**, 1792 (2008).

[64] B. Luk'yanchuk, N. I. Zheludev, S. A. Maier, N. J. Halas, P. Nordlander, H. Giessen, and C. T. Chong, Nat. Mater. **9**, 707 (2010).

[65] R. D. Artuso and G. W. Bryant, Nano Lett. **8**, 2106 (2008).

[66] K. Foster and J. Schepps, J. Microw. Power **16**, 107 (1981).

[67] S. Mallawaarachchi, M. Premaratne, S. D. Gunapala, and P. K. Maini, Phys. Rev. B **95**, 155443 (2017).